Thermodynamic Stability and Anisotropic Fluctuations in the Cylinder-to-Sphere Transition of a Block Copolymer

Chang Yeol Ryu[†,‡] and Timothy P. Lodge[*,§]

Department of Chemical Engineering & Materials Science and Department of Chemistry, University of Minnesota, Minneapolis, Minnesota 55455-0431

Received June 8, 1999; Revised Manuscript Received August 13, 1999

ABSTRACT: The stability and fluctuations of the cylinder (C) and sphere (S) morphologies in the vicinity of the C and S equilibrium have been examined for a poly(styrene-*b*-isoprene-*b*-styrene) triblock copolymer by rheology, small-angle X-ray scattering (SAXS), and transmission electron microscopy (TEM). The spinodal temperatures of the C and S phases, T_s^C and T_s^S, and the equilibrium (coexistence) temperature, T_{OOT}, have been determined by rheological measurements during thermal cycles over a wide range of heating and cooling rates. In the limit of high heating and cooling rates, T_s^C and T_s^S were determined as 202 ± 2 and 183 ± 3 °C, respectively. From the transitions at low heating and cooling rates, T_{OOT} was determined as 196 ± 1 °C. The metastability window of the S phase, $|T_s^S - T_{OOT}|$, was wider than that of the C phase, $|T_s^S - T_{OOT}|$, due to the osmotic barrier for merging spheres for the S → C transition. Prior to the C → S transition, a rheological signature of the fluctuations in the C phase was observed over a temperature interval 20 °C below T_{OOT}. The elastic shear modulus along the cylinder orientation, $G'_{||}$, starts to increase with temperature at about 176 °C. This region of $dG'_{||}/dT > 0$ is attributed to the pretransitional fluctuations in the C phase. TEM on the annealed samples at different temperatures provided real space images of various steps during the transition. TEM images from the sample annealed at 183 °C displayed many grains of undulating cylinders and supported the correlation between the anisotropic fluctuations and the rheological signature of $dG'_{||}/dT > 0$. The symmetry of the anisotropic fluctuations in the C phase was characterized as twinned body-centered-cubic by SAXS after annealing at 189 °C, where $dG'_{||}/dT > 0$.

Introduction

Block copolymers self-assemble into a variety of ordered structures and are model systems to investigate the structural and dynamic response of microstructured soft materials.[1−3] A rich array of periodic morphologies are accessible by both thermotropic and lyotropic order−order (OOT) and order−disorder transitions. Because the periodicity of each microphase is set by the macromolecular dimensions, analysis is conveniently performed by small-angle X-ray scattering and electron microscopy. Furthermore, because dynamics on time scales longer than those of the longest chain relaxation time correlate with the state of order, rheological experiments at low frequencies are sensitive to structural transitions.

It is known that block copolymers can develop long-lived transient or metastable structures during an order−order transition, because of energetic barriers combined with sluggish molecular motion.[4,5] There have been rather few experimental investigations of stability limits and anisotropic fluctuations of an ordered block copolymer phase.[6−8] This paper presents such a study for a poly(styrene-*b*-isoprene-*b*-styrene) triblock copolymer melt undergoing the reversible thermotropic cylinder-to-sphere (C → S) OOT. Rheological experiments were performed to map out the equilibrium (coexistence) temperature, T_{OOT}, as well as the spinodal temperatures, T_S, of the C and S phases. The structural evolution of the C → S transition is theoretically anticipated by Laradji et al.[9,10] and Qi and Wang[11] to proceed via anisotropic fluctuations with cubic symmetry, i.e., through periodic peristaltic undulations in the cylinder diameters. The presence of such anisotropic fluctuations with cubic symmetry in the C phase is confirmed by rheology, transmission electron microscopy (TEM), and small-angle X-ray scattering.

Background

There have been two approaches to the theoretical study of the stability/metastability of ordered phases in block copolymer melts: the Ginzburg−Landau theory (GLT) by (i) Qi and Wang[5,12,13] and (ii) Goveas and Milner[14] and the self-consistent mean-field theory (SCMFT) by Laradji et al.[9,10] Qi and Wang[5,12,13] calculated the limit of stability in the mean-field phase diagram by monitoring a time change in the order parameter after a thermodynamic jump (i.e., in temperature or χN, where χ is the interaction parameter and N is the degree of polymerization) from one phase into another; the amplitude of the least stable mode diverges as the system approaches the spinodal. The duration of transient or metastable structures was calculated for different quench depths, and the boundary of metastability (spinodal line) was estimated when this duration ≈ 0. Goveas and Milner[14] extended the mean-field phase diagram up to $\chi N \approx 30$ and $0.2 < f < 0.8$, including the lamellar-cylinder spinodal lines, to study the difference in the metastability window width between L and C phases in the vicinity of the L → C transition. They also considered the dynamic problem of an interfacial front propagating between two phases that are close to coexistence and showed that the velocity of the propagating interface is linearly proportional to the distance (in χN) from coexistence.

* Author for correspondence.
† Department of Chemical Engineering & Materials Science.
‡ Current address: Materials Research Laboratory, UCSB, Santa Barbara, CA 93106.
§ Department of Chemistry.

10.1021/ma990914+ CCC: $18.00
Published on Web 10/01/1999

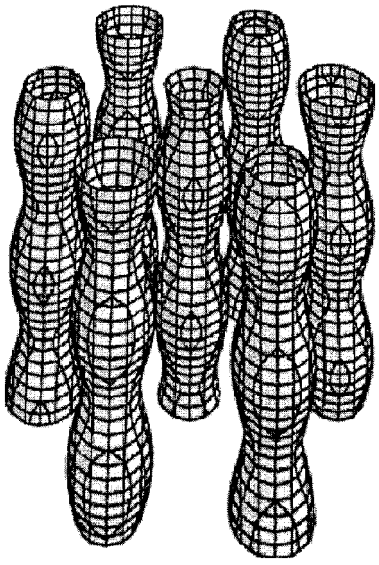

Figure 1. Illustration of the anisotropic fluctuations of the C phase prior to the C → S transition, following ref 8.

Laradji and co-workers calculated the diblock copolymer phase diagram including the spinodal boundaries (stability limits) enclosing each ordered phase in the weak-segregation regime ($10.495 \leq \chi N \leq 11.2$).[9,10] From the analysis of the eigenvalues of density−density correlation functions, the stability of each phase could be determined. There are two unrelated spinodal lines (inner and outer lines) for both C and S phases, whereas the L phase has only one (outer) spinodal line. For example, the inner spinodal line of C represents the stability limit of metastable C in the L phase for the C → L transition, whereas the outer line represents this in the S phase for C → S. The predicted phase diagram also shows metastability window differences in the vicinity of order−order transitions between two phases. For example, the metastability window of C in S prior to the C → S transition is always smaller than that of S in C prior to S → C.

A theory of anisotropic composition fluctuations has been developed by Shi et al.[15] Because a compositional periodicity provides a certain symmetry in any ordered phase, the compositional fluctuations should imitate the symmetry of the ordered structure in response to a change in thermodynamic state from stable to metastable (or unstable). The fluctuation was formulated by Shi et al. as the Gaussian deviation from the mean-field solution, and this deviation term is included in the single chain partition function to produce a band of eigenvalues of the density−density correlation function.[9,10] The most probable symmetry for anisotropic fluctuations is deduced from the signs of the eigenvalues.

The anisotropic fluctuation in C involves alternating pinching and bulging of the cylindrical domains on heating (decreasing χN), as illustrated in Figure 1. When a block copolymer in C is taken into the region between the outer spinodal line of C and the coexistence line of C and S, the pinching and bulging of cylinders into spheres was shown to be the dominant fluctuation mode. When block copolymers undergo C → S, the fluctuations possess the symmetry of S prior to the final transformation into the S phase. Similarly, when a block copolymer in C is taken into the region between the inner spinodal line of the C phase and the coexistence line of C and L, the merging of the cylinders into lamellae is the dominant fluctuation mode. Experimentally, the real space representation of anisotropic fluctuations should closely be related to TEM images. Because of the slow dynamics, the transient morphologies in the phase transitions of block copolymers can advantageously be captured by rapid quenching and TEM.[16] However, because TEM examines a small sample section, it does not provide sufficient information to characterize degenerate fluctuation modes, if there are any. For example, the fluctuations in C are predicted to reflect two degenerate modes of cubic symmetry (i.e., twinned body-centered cubic (bcc)).[11] Therefore, the reciprocal space representation is essential to describe the degenerate modes and can directly be explored by small-angle scattering experiments.

The C → S transition of asymmetric diblock copolymers has been studied experimentally by Koppi et al.[17] and Sakurai et al.[18,19] on poly(ethylenepropylene)−poly(ethylethylene) (PEP−PEE) and polystyrene−polyisoprene (PS−PI), respectively. Both systems[17,19] exhibited the same epitaxial relationship between the two morphologies: the cylinder axis coincided with the ⟨111⟩ direction of the bcc lattice, and $d^{C}_{100} \cong d^{S}_{110}$. Pretransitional fluctuations in the C phase have been proposed by Koppi et al.[17] and Kim et al.[20] Both studies postulated undulating cylinders as an intermediate structure prior to the C → S transition. For a nonionic surfactant solution, Sakya et al.[21] also proposed that the C → S transition proceeds via a column of quasispherical micelles on a bcc lattice.

Rheological studies on the stability and metastability of block copolymer ordered structures have been performed by Hajduk et al.[4] on PEP−PDMS diblock copolymers in the vicinity of the coexistence temperature between lamellar (L) and gyroid (G) phases. The transition temperature for the L → G transition shifts to lower temperature as the heating rate decreases, whereas that for the G → L transition is almost unaffected by the use of different cooling rates. Therefore, the metastability window of L in the L → G transition is much wider than that of G in the G → L transition. This experimental result could not be compared with theoretical prediction so far, because spinodal lines for the G phase have not been calculated. Recently, Almdal et al. investigated the anisotropic fluctuations of the L phase in the L → G transition by small-angle neutron scattering (SANS).[6]

Modulated morphologies, which are related to anisotropic fluctuations, have experimentally been reported in the vicinity of order−order and order−disorder transitions by a combination of rheology, TEM, SAXS, and SANS. These observations can be categorized as follows: (1) Modulation in a metastable or long-lived nonequilibrium morphology during a thermotropic structural evolution.[6,7,17,22−24] For example, bcc spheres and modulated layers (ML) have been identified as metastable intermediates for the C → disorder (D) by Bates et al.[24] and the L → C transition by Hajduk et al.,[23] respectively. (2) Modulation in a transition from a vitrified (nonequilibrium) to an equilibrium morphology upon annealing at a temperature above the glass-transition (T_g) temperature.[25] For example, Sakurai et al.[25] reported the existence of ML as a kinetic intermediate from a vitrified C phase to the equilibrium L phase by annealing a block copolymer above T_g of both blocks. The vitrified C phase was manipulated by solution casting a block copolymer from a selective solvent. (3)

Modulation instability under shear during the transition into the disordered state.[26]

Experimental Section

Materials. A poly(styrene-*b*-isoprene-*b*-styrene) triblock copolymer, denoted SIS-120, with block molecular weights of 1×10^4, 1×10^5, and 1×10^4, respectively, was provided by Dr. D. Handlin (Shell Development Co.) The polydispersity index was less than 1.06. A high degree of uniaxial cylinder orientation in SIS-120 was achieved by imposing a large strain amplitude ($\gamma_o = 0.5$ or 1.0) reciprocating shear ($w = 1$ rad/s) for 90 min under a nitrogen atmosphere at 170 °C, a temperature intermediate between the styrene T_g and T_{OOT}. The shearing device designed by Koppi et al.[17,27] was used for the alignment. The samples were sandwiched between two Teflon sheets that had been mounted on two temperature-controlled brass blocks. The sample thickness (typically 1 mm) was varied by use of a metal spacer. After good contact was made between the sample and Teflon sheets for a given thickness, the position of the stationary brass block was fixed and the spacers were taken out. The chamber was purged by several repetitions of vacuum, followed by the addition of nitrogen prior to the shear alignment.

Rheology. Dynamic viscoelastic measurements were performed on a Rheometrics solids analyzer (RSA II) operated in oscillatory shear mode. Rectangular samples were prepared prior to analysis by pressing the polymer in a mold at 150 °C. The samples were mounted into either a 0.5 or 1 mm gap shear sandwich. Temperature was controlled to within ±0.2 °C between 50 and 240 °C using a thermally controlled nitrogen purge. Because the temperature control of the RSA-II is achieved by blowing nitrogen gas through a heated coil and the temperature is measured by the thermocouple contacting the outer surface of sandwich holder, a calibration was done to quantify the temperature gradient built up in the sandwich holder. The calibration is especially important in the temperature correction of the temperature sweep experiments at high heating and cooling rates, and the results of the temperature calibration will be described later in the Results and Discussion section. All dynamic measurements were conducted at a small strain amplitude ($\gamma_0 \leq 0.02$) to access (or at least approximate[28]) the linear viscoelastic regime.

Small-Angle X-ray Scattering. SAXS experiments were conducted as follows. Cu Kα X-rays ($\lambda = 1.54$ Å) were generated by a Rigaku RU-200BVH rotating anode equipped with an 0.2×2 mm microfocus cathode and Franks mirror optics. 2D SAXS patterns were recorded by a 1024×1024 pixel area detector (Siemens) at the end of an evacuated flight tube. The sample-to-detector distance was fixed at 2.26 m for most experiments. The raw data were corrected to account for the spatial distortion of the detector surface. Samples were placed inside an evacuated chamber with an X-ray-transparent window (Kapton). Temperature was controlled over the range −30 to +260 °C by using electrical heating fingers that are embedded in the housing of sample holder and a water-cooled unit that is in partial contact with the housing.

Transmission Electron Microscopy. TEMs of SIS-120 were taken after annealing for a few minutes at the desired temperature, followed by rapid quenching by immersion in liquid nitrogen or ice water to preserve the microstructure at the annealing temperature. Although a thin film of nitrogen gas surrounds the initially hot sample and reduces the heat-transfer efficiency for the liquid nitrogen quenching, we did not observe any significant difference in the results between quenching in ice water and liquid nitrogen. Because T_g for the PS domains (ca. 100 °C) is much higher than room temperature and the molecular relaxation times associated with the triblock architecture are long, the annealed morphologies are readily preserved after a rapid quenching. After being cryomicrotomed at −110 °C with a Reichert Ultracut to provide 70 ± 10 nm thick films, the PI microdomains were stained selectively by OsO_4 vapor above an aqueous solution (4% OsO_4) for 5 ± 2 h. Therefore, the PI domains appear dark and PS domains appear bright in the TEM images. TEM samples were placed on top of a copper grid (400 mesh), and the grid was placed in the path of the electron beam inside an evacuated chamber. Images were obtained with a JEOL 1210 TEM operating in bright-field mode at a voltage of 120 kV. The TEM images were taken from more than 10 different locations on the same specimen to check for reproducibility.

Results and Discussion

The presentation of the results is divided into two parts. First, we describe the determination of the C/S coexistence temperature and the associated stability limits for SIS-120, as revealed by TEM, rheology, and SAXS. Some of the rheological features of the C → S transition were described previously, when the properties of SIS-120 were compared in detail with those of a compositionally matched diblock copolymer.[29] Second, we demonstrate the existence of anisotropic fluctuations with cubic symmetry in the stable cylinder phase. A preliminary account of these results has recently been given.[7]

Stability of the Cylinder and Sphere Phases. Prior to shear orientation, SIS-120 is in a quenched cylindrical morphology, and an isotropic SAXS pattern is observed. After the alignment protocol, a very high degree of orientation of the cylinder orientation was identified by TEM and SAXS. The hexagonal packing of the PS cylinders in the PI matrix is shown by TEM in Figure 2a, after the material was sectioned normal to the shear direction. A uniaxial orientation of cylinders may be identified in Figure 2b, when the aligned SIS-120 was sectioned normal to the shear vorticity direction. The area shown in each TEM image is on the order of 1 μm^2, and the section is very thin; therefore, the information on cylinder packing and orientation is limited to local regions. To examine the degree of orientation on a more macroscopic scale, SAXS is appropriate because it represents an ensemble average over the cross-sectional area of the X-ray beam, with a diameter of ca. 0.5 mm. In Figure 3 many higher order peaks, up to the reflections from the family of (400) planes in the hexagonal lattice, are present in the SAXS pattern when the X-rays were incident along the shear direction. This confirms that excellent long-range order was induced in the C phase by the shear alignment.

A TEM image of the bcc sphere phase is shown in Figure 2c, obtained after annealing an aligned specimen at 210 °C for 5 min. The spheres are very well arranged in the distorted hexagonal array that corresponds to the (110) plane of the bcc lattices. The (100) plane of C becomes the (110) plane of S, and the ⟨111⟩ direction of S is parallel to the cylinder axis, after an epitaxial C → S transformation. This matching between the orientation of cylinders and the ⟨111⟩ direction of bcc spheres was previously described by Koppi et al.,[17] Sakurai et al.,[19] and Sakya et al.[21] The spheres in Figure 2c appear fuzzier than the cylinder cross sections in Figure 2a due to the projection of the three-dimensional curved interface in the former.

Having established that well-oriented C and S morphologies exist at the appropriate temperatures, we now determine the associated equilibrium (coexistence) and stability limit temperatures. Figure 4 shows a schematic illustration of the stable and metastable regions of the C and S phases in the vicinity of the C/S equilibrium. Different rates of heating and cooling can be employed in rheology experiments at a low fixed frequency to estimate the spinodal temperatures of the C and S phases, as well as the coexistence temperature, because

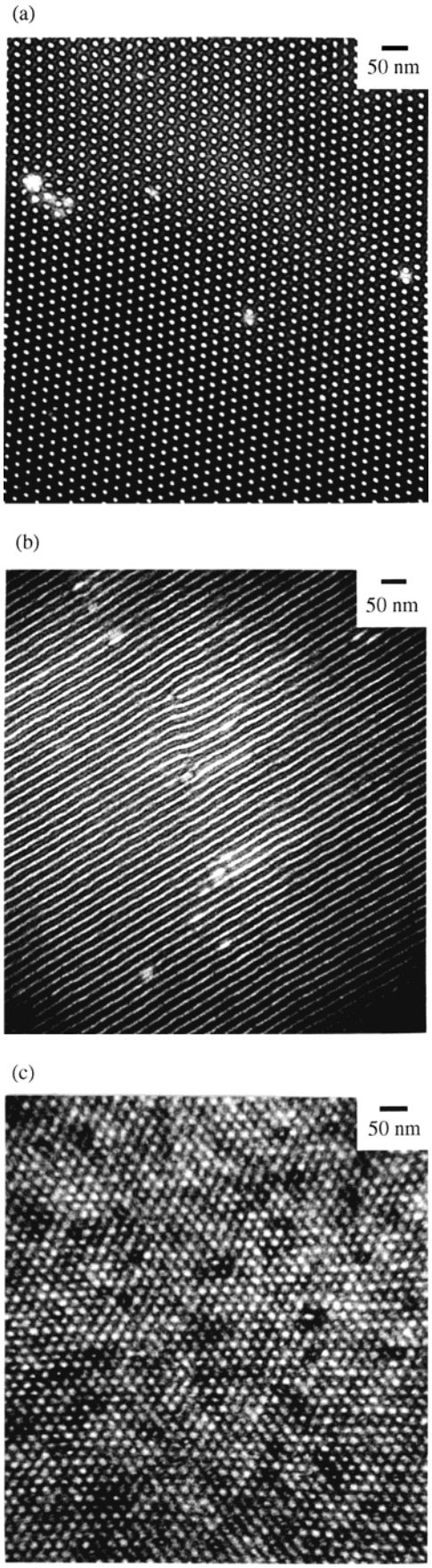

Figure 2. TEM micrographs of aligned samples with the section normal to (a) the shear axis and (b) the vorticity axis after being annealed at 173 °C for 10 min and (c) at 210 °C for 5 min.

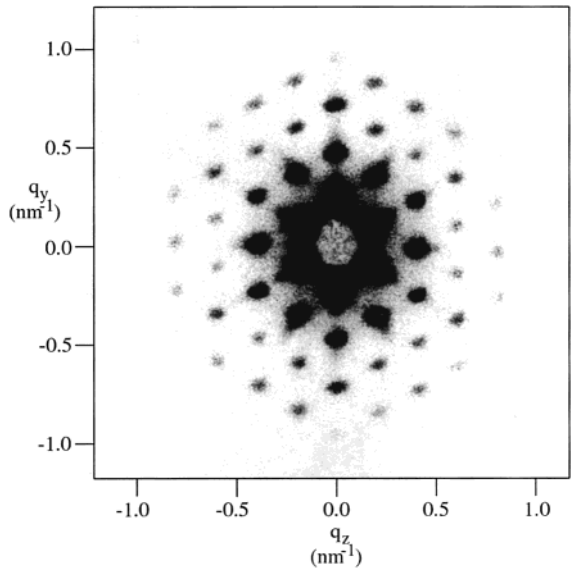

Figure 3. SAXS diffraction pattern from the shear-aligned SIS-120 with X-rays incident along the shear direction (*x*). The *y* and *z* directions represent the shear gradient and vorticity direction, respectively.

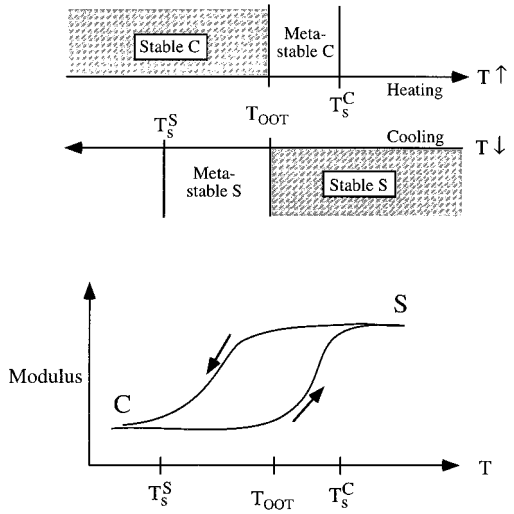

Figure 4. Schematic diagram to illustrate regions of stable and metastable phases in the vicinity of the C/S equilibrium.

the modulus in quite sensitive to the state of order. Associated with this first-order transition is a hysteresis loop, also illustrated in Figure 4. For example, the C → S transition occurs upon heating and is indicated by a marked increase in modulus over a certain narrow temperature interval. For a vanishing heating rate, this interval would coincide with the thermodynamic coexistence temperature, T_{OOT}, whereas as the rate is increased, this temperature interval will move toward the stability limit of the cylinders, T_s^C. Similarly, upon cooling at a finite rate, the S → C transition will take place at a temperature below coexistence but above the stability limit of the spheres.

There are two dynamic moduli in an oriented C phase, $G'_{\parallel}$ and $G'_{\perp}$,[29] where the subscripts denote shearing along or transverse to the cylinder axis, respectively. The temperature dependence of the low-frequency dynamic shear elastic modulus parallel to the cylinder axis, $G'_{\parallel}(T)$, is employed for the rheological detection of the C → S transition, because it displays the more remarkable change at the C → S transition. Figure 5

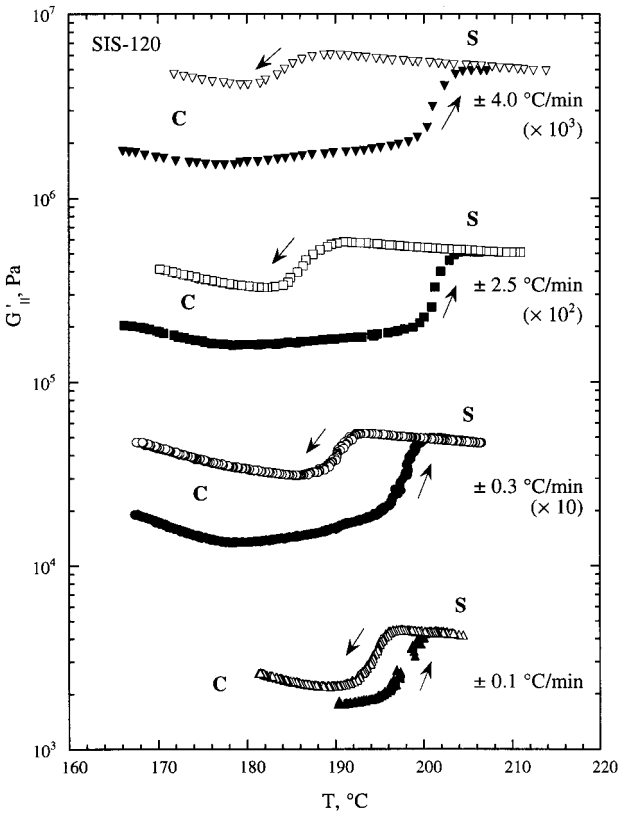

Figure 5. Temperature dependence of the dynamic elastic shear modulus $G_{||}'(T)$ ($\omega = 1$ rad/s, $\gamma_o = 4\%$) showing both heating (filled symbols) and cooling (open symbols) cycles at four different scan rates.

shows traces of $G_{||}'(T)$ for heating and cooling cycles at four different rates. As noted above, the C → S transition occurs at temperatures between T_{OOT} and T_s^S, whereas the S → C transition occurs at temperatures between T_{OOT} and T_s^S. A distinct hysteresis loop is observed, and the width of the loop decreases with decreasing $|\partial T/\partial t|$. It is interesting to note that the temperature of the C → S transition is less affected by a change in heating/cooling rates than the temperature for the S → C transition. It should also be pointed out that the modulus does not recover to its original value after the cycle, because once the material is in the S phase some memory of the original C orientation is lost. This phenomenon has been studied in more detail by Kim.[30]

The results for the transitions at different heating and cooling rates are summarized in Figure 6. The transition temperatures are taken as the midpoint of the temperature range over which the modulus undergoes a steep rise or descent, and the error bars correspond to the range itself. The C → S transition temperature reaches an asymptotic value and becomes more or less independent of heating rate at high rates. Therefore, T_s^C is determined to be 202 ± 2 °C. The S → C transition temperature depends more strongly on the cooling rate, and T_s^S is estimated to be about 183 °C (or less). Thus, T_s^C is determined more precisely than T_s^S, because the transition temperature is independent of further increase in heating rate above 3 °C/min. Higher heating and cooling rates are precluded due to heat-transfer limitations. Low heating and cooling rates are important for the determination of the C and S coexistence (equilibrium) temperature T_{OOT}, which is calculated to be 196 ± 1 °C by interpolation.

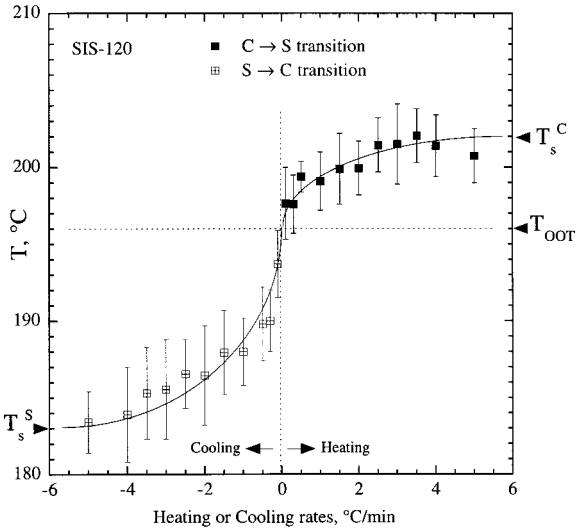

Figure 6. Temperature scan rate dependence for the C → S transition on heating and the S → C transition on cooling from rheology. The error bar represents the range of temperature over which dynamic the modulus changes abruptly at the order−order transition for a given scan rate.

It is necessary to comment on heat-transfer limitations in determining the exact temperature of the sample in the RSA-II at high heating and cooling rates. Because the RSA-II is equipped to measure the temperature of the outer surface of the sandwich holder, it is essential to consider the temperature difference between the sample inside the holder and the RSA-II monitor. Accordingly, the temperature of the sample was measured independently and directly using a thermocouple embedded in the sample (in the absence of shear) at various heating and cooling rates. The data presented here represent the actual sample temperatures, corrected for the rate-dependent difference between the instrument reading and the in situ probe.

In general, the metastability window of the S phase in the S → C transition is predicted to be much wider than that of the C phase in the C → S transition (i.e., $|T_s^C - T_{OOT}| < |T_{OOT} - T_s^S|$). From the theoretical phase map of Laradji et al.,[9,10] we can estimate the relative width of the metastability window between the C and S phases with $0.4 \le f \le 0.6$ as follows:

$$\left|\frac{(\chi N)_s^S - (\chi N)_{OOT}}{(\chi N)_s^C - (\chi N)_{OOT}}\right| = 4 \pm 2 \qquad (1)$$

The estimate is restricted to this composition window because the calculations were limited due to substantial increase in calculation time as the composition deviates further from symmetry. From Figure 6, the coexistence and spinodal temperatures of SIS-120 were estimated, and therefore, the ratio of metastability window of the S and C phases for SIS-120 can be calculated, using $\chi = 33/T - 0.0228$ (determined on the basis of a styrene segment reference volume[31]).

$$\left|\frac{(\chi N)_s^S - (\chi N)_{OOT}}{(\chi N)_s^C - (\chi N)_{OOT}}\right| = 2.3 \qquad (2)$$

Given the difference in composition between the calculation and the experiment, plus possible differences due to the triblock architecture, we may conclude that the

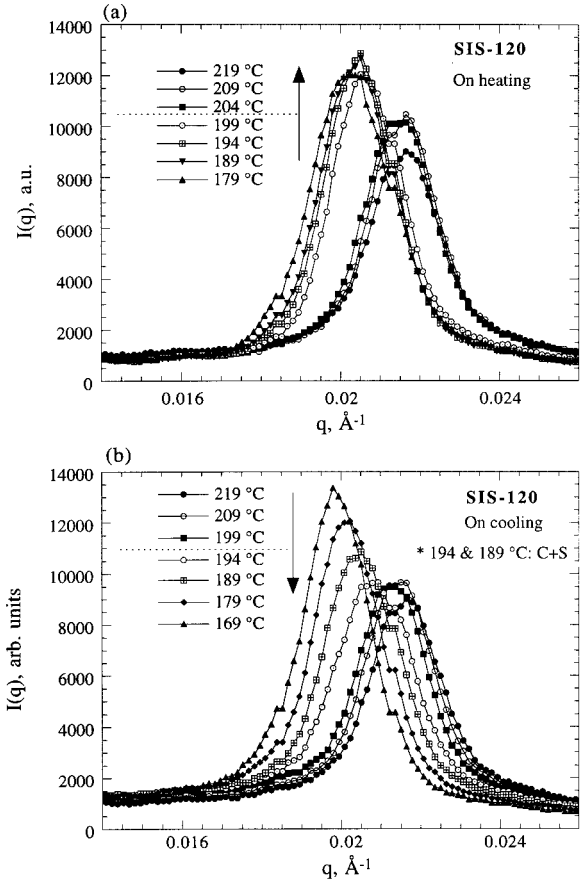

Figure 7. Temperature dependence of SAXS profiles of unoriented SIS-120 around $q = q^*$ on (a) heating and (b) cooling. Sample was annealed for 20 min at each temperature prior to X-ray exposure.

results are in at least qualitative agreement with theory. This metastability difference is attributable to the difference in the energy barrier between the C → S and S → C transitions. The merging of spheres (S → C) has a larger barrier than the pinching-off and bulging of cylinders (C → S), due to the osmotic repulsion between the PI coronae in the S morphology.

The asymmetry in the window of metastability about the coexistence temperature is also evident in the temperature evolution of the structure factor. SAXS patterns around q^* for SIS-120 at different temperatures are shown in Figure 7 on (a) heating and (b) cooling through the transition. At each temperature, the material was annealed for 20 min prior to a 10 min exposure in the X-ray beam. An abrupt increase in q^* was observed for the C → S transition on heating (Figure 7a) above 200 °C, whereas an apparently continuous decrease in q^* is shown for the S → C transition on cooling (Figure 7b). This progressive decrease in q^* on cooling is due to peak broadening from the persistence of metastable S and the concomitant slow refinement of the C structure. In contrast, $I(q)$ on heating gives the impression of a sharp transformation of C to S. However, it should be noted that the curve at 199 °C in Figure 7a falls close to the lower temperature traces from C, even though the temperature lies above T_{OOT}. This is consistent with Figures 5 and 6, where heating at 0.1 °C/min (which is comparable with the heating rate for the SAXS measurements) does not produce the final S structure until T exceeds 200 °C.

The coexistence of stable C and metastable S phases on cooling is apparent in the higher order reflections

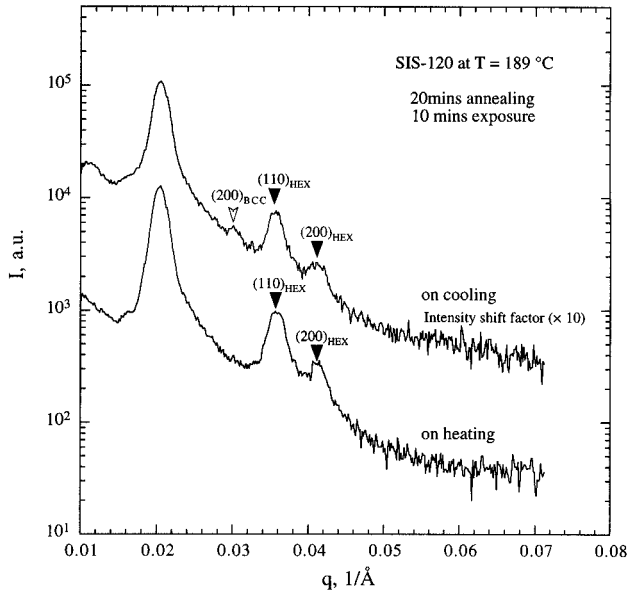

Figure 8. Azimuthally averaged SAXS intensity at 189 °C on (a) heating and (b) cooling. Note that the $(200)_{bcc}$ reflection only exists on cooling due to the coexistence of cylinders and the metastable bcc spheres.

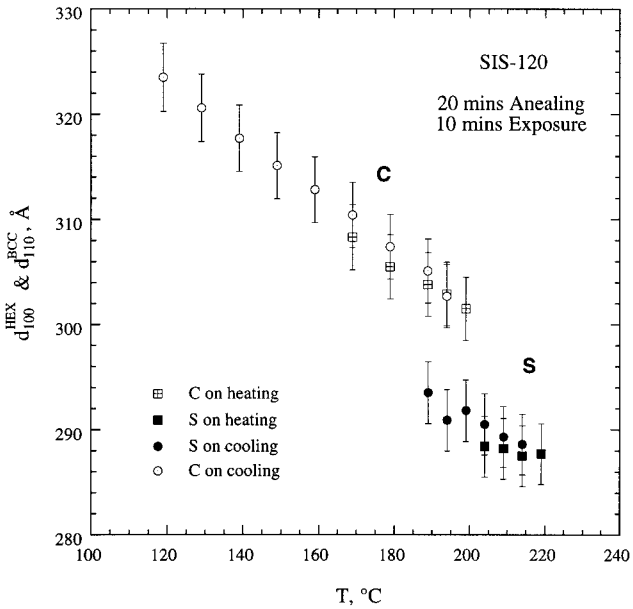

Figure 9. Temperature dependence of domain spacing on heating and cooling. Sample was annealed for 20 min at each temperature prior to SAXS. Note that C and S coexist at 194 and 189 °C on cooling, and the domain spacing for the C and S phases was calculated from $(3)^{1/2}q^*$ and $(2)^{1/2}q^*$ peaks, respectively.

from an unoriented sample. SAXS patterns at the same temperature of 189 °C on heating and cooling are compared in Figure 8. The C phase is stable and gives clear reflections of q^*:$(3)^{1/2}q^*$:$(4)^{1/2}q^*$ on heating. However, on cooling a reflection at ca. $(2)^{1/2}q^*$, which is indicative of a cubic structure, persists during 20 min annealing at 189 °C. The temperature dependence of the principal lattice spacing d ($=2\pi/q^*$) for the C and S phases is shown in Figure 9. d_{100}^{HEX} and d_{110}^{bcc} were calculated from the high-order reflections at $(3)^{1/2}q^*$ and $(2)^{1/2}q^*$, respectively, after subtracting power-law fitted baselines from the intensity. This way of calculating d instead of using the first-order peak q^* is especially useful to resolve two different domain spacings of C and

S when the C and S phases coexist. There is a decrease in d of about 4% (i.e., an increase in q^*) at the C → S transition. This distinct increase in q^* for both polymers upon the C → S transition contrasts with previous studies,[17,19] where little change in the spacing was noted. However, it is at least qualitatively consistent with the chain stretching predictions in various ordered structures at weak segregation by Olvera de la Cruz.[32] Compared to the chain conformation in the disordered state, chains are predicted to be more stretched and contracted in C and S, respectively, by modifying Leibler's mean-field theory[33] with the concentration fluctuations via a Hartree analysis. Furthermore, it was pointed out by Matsen and Bates that conformational asymmetry can play an important role.[34] When the minor component has the larger statistical segment length, as was the case for Koppi et al.,[17] little change in q^* at this OOT is predicted. On the other hand, the domain spacing between C and S is predicted to change by about 10% at $\chi N = 30$,[34] which is at least in qualitative agreement with the observed change for SIS-120. Recently, Sakamoto et al. also observed a similar domain spacing mismatch for the C → S transition of a PS−PI−PS triblock copolymer.[35] The difference in q^* has important implications for the epitaxial nature of the C → S transition. In particular, it is not possible for perfect epitaxy to exist over macroscopic length scales without some distortion to accommodate the q^* mismatch. Furthermore, the resulting bcc structure should actually be twinned, which further complicates the transformation. Possible evidence of the effects of this mismatch will be presented in the following section.

Anisotropic Fluctuations in the Cylinder Phase. The experimental results in this section focus on the rheological, TEM, and SAXS signatures of anisotropic fluctuations in C. The temperature dependence of $G'_{\|}(T)$ for SIS-120 in C is nonmonotonic, as shown in Figure 10a. There is a temperature interval from about 175 to 195 °C over which the modulus increases, prior to the abrupt increase that signals the OOT; this is emphasized by the dotted box. In contrast, $G'_{\perp}(T)$ and $G'_{R}(T)$ decrease monotonically with increasing temperature over the same region, as does $G''(T)$ for all three measurement geometries (Figure 10b). This phenomenon was consistently observed for both higher and lower heating rates (see Figure 5). This feature was previously postulated to reflect pretransitional fluctuations[6,17,20,29] in the C structure, and in this section we present additional evidence that confirms this interpretation. The low values of $G'_{\|}(T)$ relative to $G'_{\perp}(T)$ and $G'_{R}(T)$ were attributed to the ability of the unentangled styrene blocks to relax stress by diffusing along the cylinder axis. In this scenario, fluctuations in the cylinders, i.e., peristaltic undulations in the cylinder diameter, act to impede this mode of relaxation. As temperature increases toward the OOT, the amplitude and thus the effect of these fluctuations grow.

The frequency dependence of $G'_{\|}(T)$ is shown in Figure 11 for several temperatures within C. The data have been superposed by shifting along the frequency axis to match the behavior at high frequencies. Time−temperature superposition (TTS) apparently holds for 137 °C ≤ T ≤ 167 °C but fails at low frequencies when T = 177 and 187 °C. Thus, the temperatures where this failure of TTS is observed correspond to the window where there is a positive slope of $dG'_{\|}/dT$. Although TTS is not expected to be valid in block copolymers in general, this kind of abrupt change in the shape of modulus versus frequency is typically indicative of some change in structure.

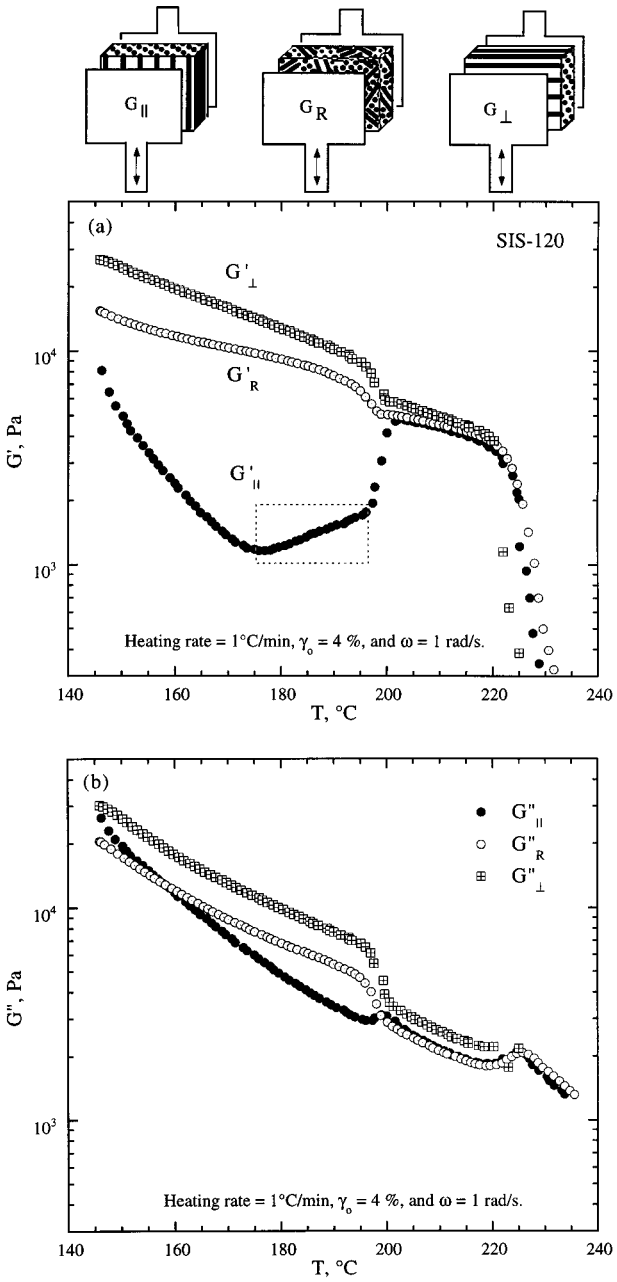

Figure 10. Temperature dependence of three dynamic (a) elastic and (b) viscous shear moduli with different initial cylindrical orientations at $\omega = 1$ rad/s, $\gamma_o = 4\%$, and a heating rate of 1 °C/min. To illustrate how $G_{\|}$, G_R, and $G_{\perp}$ are defined in a simple shear, a schematic diagram is also provided. The reciprocating arrows indicate the shear direction for the viscoelastic measurement.

Fluctuations in the cylinder microstructure are evident from TEM images that were obtained after the annealing of SIS-120 at 183 (Figure 12a,b) and 193 °C (Figure 12c), where $dG'_{\|}/dT > 0$. The annealed and quenched samples were sectioned normal to the vorticity axis to monitor any change in the side view of the cylinders. These results may be compared with those of Figure 2b, which show aligned cylinders of SIS-120 after annealing for 10 min at 173 °C, a temperature in the regime where $G'_{\|}(T)$ decreases with increasing T (i.e., $dG'_{\|}/dT < 0$). Although some defects and wiggles in cylinder orientation are visible, the stable and highly

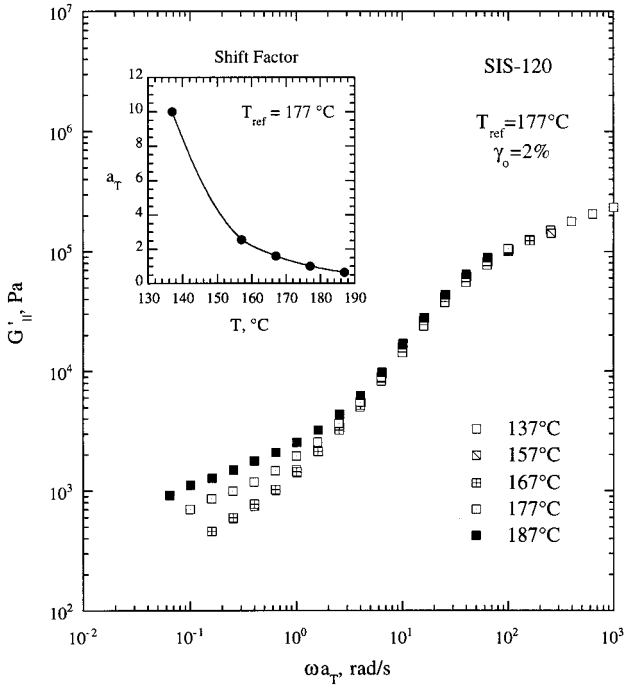

Figure 11. Time−temperature superposition (TTS) of $G'_{||}$. The apparent TTS is observed at high frequencies. The deviation from the TTS master curve at low frequencies for 177 and 187 °C is related to the onset of fluctuations prior to the C → S transition.

oriented cylinder morphology is still apparent without showing any region of undulation or fluctuation. In contrast, local development of the undulating cylinder domains in "grains" approximately 0.5 μm in extent are evident in parts a and b of Figure 12, where the sample has been annealed for 10 min at 183 °C. Close examination suggests an approximately hexagonal arrangement of elongated "droplets" in the grain, with the underlying cylindrical orientation still being preserved. The appearance of these grains is therefore correlated with the change in sign of $dG'_{||}/dT$. A "fully developed" state of undulating cylinders, with the original cylinder orientation maintained, is observed in Figure 12c, after annealing for 10 min at 193 °C. The undulation of cylinders prevails throughout the field of view for all specimens examined after annealing at 193 °C, whereas the undulation is always confined to local regions after annealing at 183 °C.

TEM gives clear evidence of the nature of the fluctuations in the stable C phase, but because each image is confined to a relatively small region of the sample, it is not possible to conclude whether the fluctuations have the bcc symmetry anticipated by theory. Consequently, we undertook to examine the SAXS patterns from the same material. A specimen of well-oriented cylinders confined between Kapton sheets was placed in the sample chamber at room temperature. Thin films of Kapton were chosen not only because they are effectively transparent to X-rays but also because they prevent samples from bending during annealing at high temperatures. The cylinder axis was oriented vertically (designated as the x direction), and the X-rays are incident along the shear gradient direction (designated as y). Qi and Wang[10] developed a reciprocal space representation of anisotropic fluctuations, which is useful in demonstrating the proposed scattering patterns from various microstructural orientations with respect to the incident beam. The suggested anisotropic fluctuation scattering pattern is demonstrated by a cross-sectional plane through the sphere in three-dimensional reciprocal space. For example, the scattering pattern with the incident beam parallel to the y axis in real space is described from the cross section with $q_y = 0$ in reciprocal space. As shown in Figure 13b, the SAXS diffraction patterns in the q_x-q_z plane ($q_y = 0$) corresponds to the shaded plane in Figure 13a.

The sample was slowly heated under vacuum from room temperature to 189 °C at approximately 1 °C/min to emulate the thermal history of the rheology experiments. Then, SAXS diffraction images (20 min exposures) were taken at successive times after the sample was annealed at 189 °C. There are distinct Bragg reflections at $\pm(3)^{1/2}q^*$ without any scattering at q^* after 1 h of annealing at 189 °C (Figure 14a). These reflections came from the periodicity given by the (110) planes in C. The four lobes around the beam stop are due to parasitic scattering, which originates from scattering at the edge of the main guard slits. After 2 h of annealing, the diffraction pattern shown in Figure 14b was observed. Two pair of faint peaks (denoted as A′, A″ and B′, B″) appeared at q^*, coexisting with the strong $\pm(3)^{1/2}q^*$ Bragg reflection. The intensity difference ΔI at q^* is obtained by subtracting the scattering intensity of Figure 14a from that of Figure 14b. In Figure 14c, the resulting plot of ΔI as a function of azimuthal angle $\tilde{y}$ clearly indicates four weak peaks: A′, A″ and B′, B″. These peaks are well-resolved and are separated by an angle of about 110° between A′ and B′ or A″ and B″. According to the theoretical study of Qi and Wang,[11] there are two pairs of weak fluctuation peaks appearing at $q = q^*$ with an angle of 110 ° between them in the scattering plane of $q_y = 0$ (Figure 13b). There are 12 points of fluctuations in three-dimensional reciprocal space, and these fluctuations are subdivided into two sets of 6 fluctuation points corresponding to two degenerate sets of the bcc fluctuations (twinned bcc) in the cylindrical morphology. Therefore, after the annealing of SIS-120 for 2 h at 189 °C, the two pairs of weak peaks in the scattering plane of $q_y = 0$ at an angle about 110 ° can be attributed to two degenerate pairs of fluctuation peaks from the anisotropic fluctuations in the cylinders possessing a twinned bcc symmetry.

There are two other possible explanations for the particular nonmonotonic temperature dependence of $G'_{||}(T)$ at $T < 200$ °C that merit consideration: (1) a slow nucleation of spheres that begins near 180 °C, followed by an abrupt transition at the stability limit of the C phase around 200 °C, and (2) a wide coexistence region between cylinders and spheres ($180 < T < 200$ °C) due to polydispersity. The former explanation is not probable, because the nucleation of spheres is not thermodynamically favorable at temperatures below the coexistence temperature of the C and S phases, T_{OOT}. As shown in Figure 6, T_{OOT} was determined to be about 196 ± 1 °C by the combination of heating (C → S) and cooling (S → C) experiments at various slow rates. The nucleation of the S phase should therefore appear only for $T_{OOT} < T < T_s^C$, where the C phase is metastable. Further evidence against hypothesis 1 comes from the rheological reversibility between the stable and undulating cylinders, shown in Figure 15. Heating and cooling traces of $G'_{||}(T)$ are compared for temperature cycles of $T_1 \rightarrow T_2 \rightarrow T_1$, where T_1 is fixed at 178 °C and T_2 is varied as 188, 198, and 203 °C. Each trace represents a measurement on a freshly shear-oriented

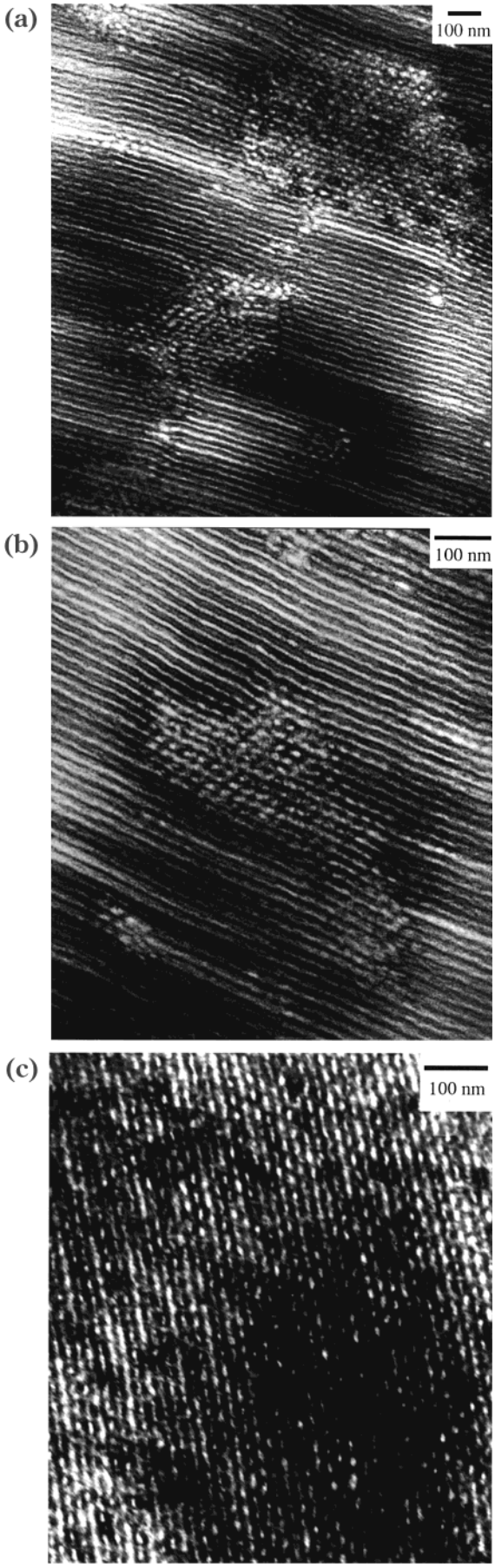

Figure 12. TEM micrographs with aligned cylinders after being annealed under vacuum at (a) and (b) 183 °C for 10 min and (c) 93 °C for 10 min. After being annealed, samples were quenched into liquid nitrogen or iced water.

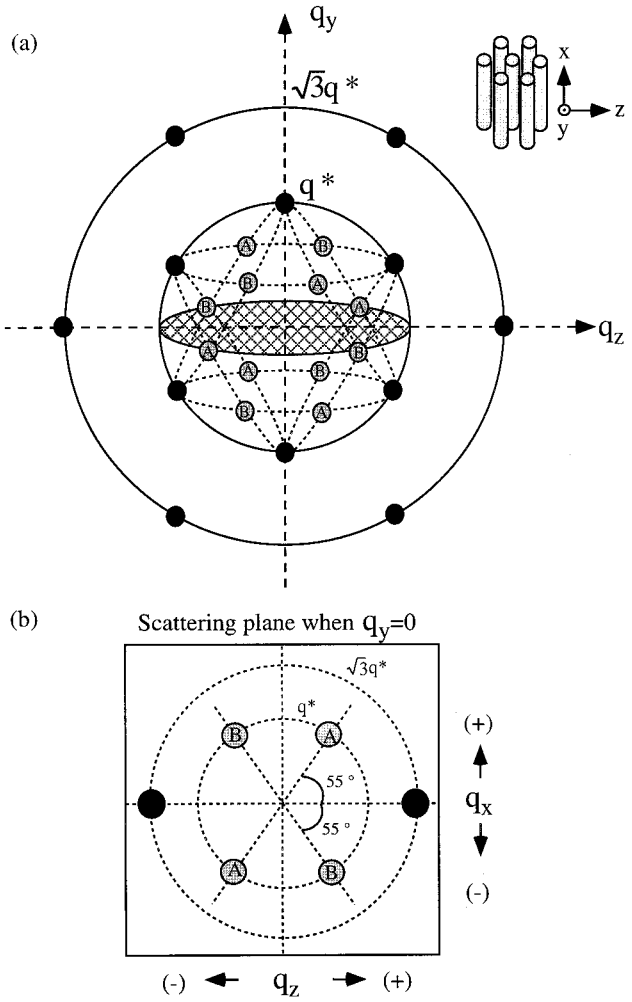

Figure 13. (a) Anisotropic fluctuation modes of the C phase in reciprocal space, where cylinders are oriented along the *x* axis. The dark spots represents Bragg reflections from the C phase, whereas the 12 gray spots show the anisotropic fluctuation mode in the twinned bcc structure (2 sets (A and B) of 6 gray spots). (b) Bragg reflections in the scattering plane where $q_y = 0$. This slice corresponds to the shaded section in part a.

specimen. For the cycle with T_2 = 188 °C, the cooling trace of $G'_{||}(T)$ overlaps exactly with the heating traces, and this indicates that the transition between the stable and undulating cylinders is completely reversible over this temperature window. If the increase in $G'_{||}(T)$ were due to the slow nucleation of stable spheres, they should persist upon cooling and the modulus would not decrease. The reversibility of the cylinder undulation is also supported by the results of frequency sweep experiments,[36] where the frequency dependence of $G'_{||}(\omega)$ and $G''_{||}(\omega)$ at 157 °C overlaps exactly both before and after being heated to 188 °C during the cycle in Figure 15. For the cycle with T_2 = 198 °C, $G'_{||}(T)$ does not retrace the heating curve upon cooling but is offset slightly. This is attributable to the loss of some orientational order of the cylinders, due to the first appearance of local regions of spheres. Because T_2 is slightly higher than T_{OOT}, the C phase becomes metastable and a bcc array of spheres should emerge. However, the time scale is much too short to allow wholesale development of the sphere phase. Once in a bcc array, there are four degenerate ⟨111⟩ axes that can transform back into the ⟨100⟩ axes of C. Thus, the deviation between the heating and cooling traces for this cycle is a measure of how much the brief interval above T_{OOT} has disrupted the memory

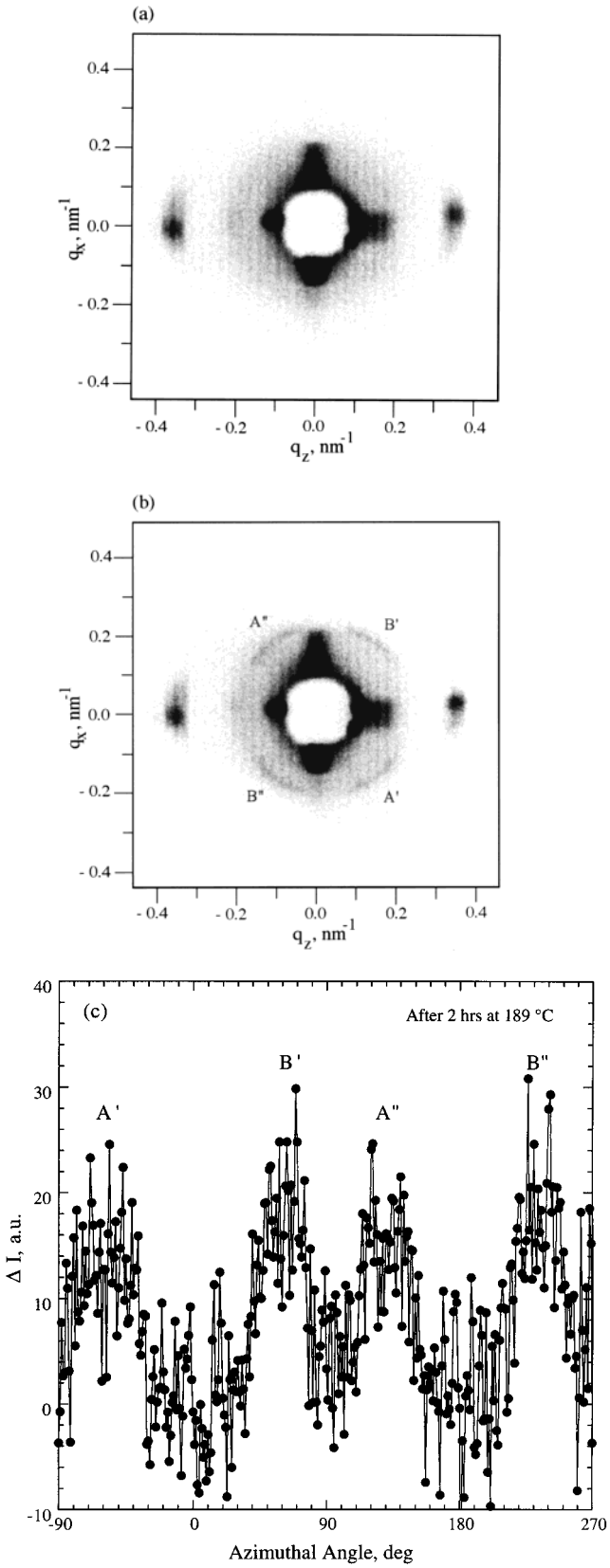

Figure 14. 2D SAXS patterns of SIS-120 after being annealed under vacuum at 189 °C for (a) 1 and (b) 2 h. The sample has been oriented prior to annealing, and the incident radiation was directed along the shear gradient direction (y axis in Figure 13). (c) SAXS azimuthal plot at $q = q^*$ for ΔI, i.e., the data from part b of this figure after the data from part a was subtracted as background.

of the prior cylindrical orientation. Finally, for the cycle with $T_2 = 203$ °C, the cooling trace of $G'_{||}(T)$ is completely different from the heating trace. Because $T_2 = 203$ °C is located in the unstable C phase (i.e., $T_2 > T_s^C$), C transforms into stable S spontaneously and the cooling trace resembles those in Figure 5, which began with well-developed S. Thus, in summary, these temperature cycle measurements indicates that the positive values of $G'_{||}/dT$ do not represent nucleation of S in a metastable C phase.

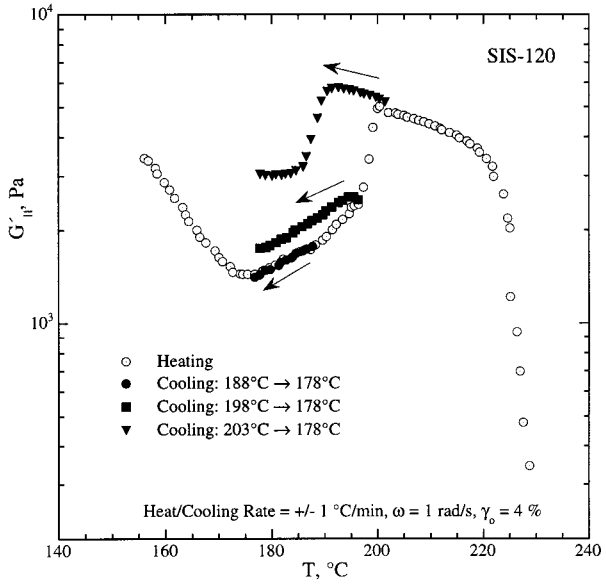

Figure 15. Temperature dependence of $G'_{||}$ ($\omega = 1$ rad/s, $\gamma_o = 4\%$) on cooling from different temperatures at a fixed temperature scan rate (1 °C/min) in a heating and cooling cycle.

Hypothesis 2, that the positive $dG'_{||}/dT$ is due to a smearing of the transition by polydispersity, can be discarded based on the following result. A deliberately polydisperse sample was prepared by blending SIS-120 with SI-60, where SI-60 is a PS−PI diblock copolymer with $M_{PS} = 10\,000$ and $M_{PI} = 50\,000$; SI-60 is thus the matched diblock copolymer for SIS-120, in that it has the same PS content and half the molecular weight as SIS-120, and undergoes the same type of the C → S transition.[29] A blend of SIS-120/SI-60 with a composition of approximately 50/50 by weight was prepared by freeze-drying from benzene solution. The sample was shear-oriented, and the dynamic moduli parallel to the cylinder axes were monitored as a function of temperature. As is evident from Figure 16, the qualitative features of the $G'_{||}(T)$ trace are exactly those observed in pure SIS-120, with the onset of an increase in $G'_{||}(T)$ with increasing temperature at 145 °C, prior to the transformation to S around 175 °C. SEC traces of the sample in the inset of Figure 16 show the polydisperse (bimodal) molecular weight distribution of this blend. Because the same behavior of $G'_{||}(T)$ is observed from this very polydisperse blend and from pure SIS-120, it is clear that molecular weight polydispersity is not the reason for the temperature region with $dG'_{||}/dT > 0$.

Finally, it is necessary to consider whether cylinder undulation is possible not only for $T_{OOT} < T < T_s^C$, where it is predicted, but also for $T < T_{OOT}$. We have correlated the nonmonotonic temperature dependence of $G'_{||}(T)$ within the C phase, i.e., $T < T_{OOT}$, with the pretransitional fluctuation of cylinders prior to the C → S transition. Theoretical studies have predicted the anisotropic fluctuations in ordered phases of block copolymers to occur in the metastable region.[5,9] Accordingly, the cylinder undulation of SIS-120 should occur

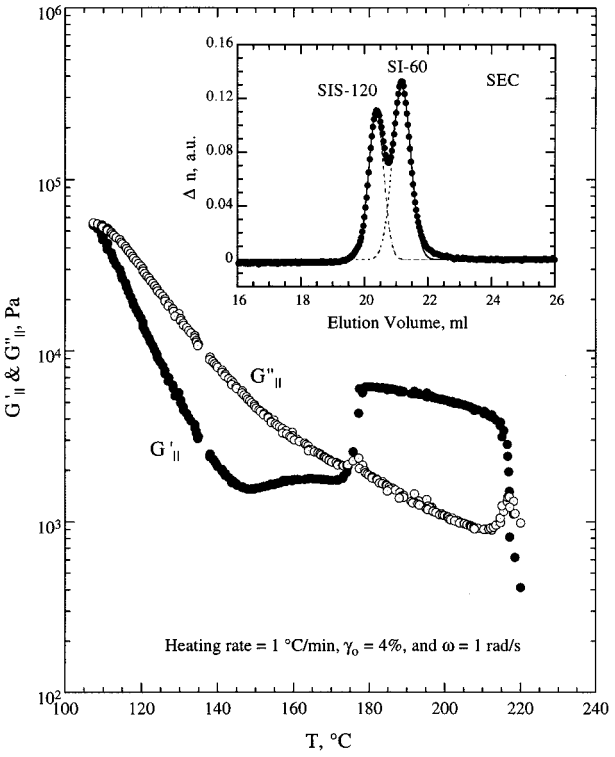

Figure 16. Temperature dependence of $G'_{||}$ and $G''_{||}$ for a 50:50 blend of SIS-120 and SI-60. SEC trace of the blend is shown in the inset to illustrate the polydisperse molecular weight distribution.

at temperatures for the metastable cylinders: 196 (T_{OOT}) $\leq T \leq$ 202 °C (T_s^C). However, the rheological signature of cylinder undulation was observed at $T \approx 176$ °C, which is 20 °C lower than T_{OOT}. This is consistent with the previous postulate of pretransitional fluctuations in the C phase before the C → S transition by Koppi et al.[17] and Kim et al.[20] from SANS and DSC experiments, respectively. We can consider the undulation amplitude $\vec{h}$, which represents the deviation of the cylinder radius from the mean. In the mean-field approximation, the modulation amplitude $\langle \vec{h}^2 \rangle$ diverges at $T = T_s^C$ and scales as follows:

$$\langle \vec{h}^2 \rangle \sim \frac{1}{|T - T_s^C|} \quad \text{when } T < T_s^C \tag{3}$$

This means that the modulation amplitude is proportional to the thermodynamic distance from the stability limit and the modulation of cylinders can exist as long as $T < T_s^C$, regardless of whether T is above or below T_{OOT}. Because the metastability window of the C phase is narrow, it is therefore plausible that there is a significant amplitude in the cylinder fluctuations at $T \leq T_{OOT}$. Although the temporal fluctuations in the cylinders with a finite amplitude $\vec{h}$ are possible, the amplitude should decay down to zero at $T < T_{OOT}$. For temperatures where the fluctuations first appear (see parts a and b of Figure 12), the fluctuations appear confined to spatial regions on the order of 0.5 μm in extent. This is attributable to the mismatch in q^* between C and S phases, which inhibits the growth of fluctuations over macroscopic distances.

Summary

SIS-120, which is a PS−PI−PS triblock copolymer with $M = 120\,000$ and $f_{PS} = 0.15$ by volume, undergoes a thermotropic OOT between hexagonally packed cylinders (C) and body-centered cubic spheres (S). There are three temperatures involved in the vicinity of the equilibrium between the C and S phases: the coexistence temperature, $T_{OOT} = 196 \pm 2$ °C, and the spinodal temperatures of the C and S phases, T_s^C and $T_s^S = 202 \pm 2$ °C and 183 ±3 °C, respectively. The metastable C phase can exist as a superheated state at $196 \leq T < 202$ °C, whereas the metastable S phase at $183 \leq T \leq 196$ °C is supercooled. The relatively wider window for the metastable S phase originates from the osmotic barrier for merging spheres and is in reasonable agreement with theoretical prediction.[9,10]

Pretransitional fluctuation of cylinders prior to the C → S transition is investigated by rheology, TEM, and SAXS. The rheological correlation with the cylinder undulations is apparent only when the shear moduli are measured parallel to the cylinder orientation. An onset of the long-lived temporal fluctuations with an induction time for nucleating a region of undulations is found at $T < T_{OOT}$, where the C phase is stable. This is mainly attributable to the slight mismatch in the periodicity between the C and S phases. Direct evidence for the undulating cylinders is shown by TEM in real space, and the twinned bcc symmetry of the anisotropic fluctuations is observed by SAXS in reciprocal space. There is an excellent agreement between theory and experiment to support the anisotropic fluctuation of cylinders in a twinned bcc symmetry by the analysis of the fluctuation peaks observed with SAXS.

Acknowledgment. This work was supported by the National Science Foundation through DMR-9528481. D. W. Giles provided assistance with the temperature calibration of the RSA-II, and M. E. Vigild contributed to the SAXS experiments. Helpful discussions with K. Almdal, D. C. Morse, A.-C. Shi, and Z.-G. Wang are appreciated.

References and Notes

(1) Bates, F. S.; Fredrickson, G. H. *Annu. Rev. Phys. Chem.* **1990**, *41*, 525.
(2) Fredrickson, G. H.; Bates, F. S. *Annu. Rev. Mater. Sci.* **1996**, *26*, 501.
(3) Hamley, I. W. *The Physics of Block Copolymers*; Oxford University Press: New York, 1998.
(4) Hajduk, D. A.; Takenouchi, H.; Hillmyer, M. A.; Bates, F. S.; Vigild, M. E.; Almdal, K. *Macromolecules* **1997**, *30*, 3788.
(5) Qi, S.; Wang, Z.-G. *Phys. Rev. E.* **1997**, *55*, 1682.
(6) Almdal, K.; Vigild, M. E.; Mortensen, K., unpublished results.
(7) Ryu, C. Y.; Vigild, M. E.; Lodge, T. P. *Phys. Rev. Lett.* **1998**, *81*, 5354.
(8) Floudas, G.; Pakula, T.; Velis, G.; Sioula, S.; Hadjichristidis, N. *J. Chem. Phys.* **1998**, *108*, 6498.
(9) Laradji, M.; Shi, A.-C.; Noolandi, J.; Desai, R. C. *Macromolecules* **1997**, *30*, 3242.
(10) Laradji, M.; Shi, A.-C.; Desai, R. C.; Noolandi, J. *Phys. Rev. Lett.* **1997**, *78*, 2577.
(11) Qi, S.; Wang, Z.-G. *Polymer* **1998**, *39*, 4639.
(12) Qi, S.; Wang, Z.-G. *Phys. Rev. Lett.* **1996**, *76*, 1679.
(13) Qi, S.; Wang, Z.-G. *Macromolecules* **1997**, *30*, 4491.
(14) Goveas, J. L.; Milner, S. T. *Macromolecules* **1997**, *30*, 2605.
(15) Shi, A. C.; Noolandi, J.; Desai, R. C. *Macromolecules* **1996**, *29*, 6487.
(16) Sakamoto, N.; Hashimoto, T. *Macromolecules* **1998**, *31*, 3815.
(17) Koppi, K. A.; Tirrell, M.; Bates, F. S.; Almdal, K.; Mortensen, K. *J. Rheol.* **1994**, *38*, 999.
(18) Sakurai, S.; Kawada, H.; Hashimoto, T.; Fetters, L. J. *Macromolecules* **1993**, *26*, 5796.
(19) Sakurai, S.; Hashimoto, T.; Fetters, L. J. *Macromolecules* **1996**, *29*, 740.
(20) Kim, J. K.; Lee, H. H.; Gu, Q.-J.; Chang, T.; Jeong, Y. H. *Macromolecules* **1998**, *31*, 4045.

(21) Sakya, P.; Seddon, J. M.; Templer, R. H.; Mirkin, R. J.; Tiddy, G. J. T. *Langmuir* **1997**, *13*, 3706.
(22) Hamley, I. W.; Gehlsen, M. D.; Khandpur, A. K.; Koppi, K. A.; Rosedale, J. H.; Schulz, M. F.; Bates, F. S.; Almdal, K.; Mortensen, K. *J. Phys. II France* **1994**, *4*, 2161.
(23) Hajduk, D. A.; Gruner, S. M.; Rangarajan, P.; Register, R. A.; Fetters, L. J.; Honeker, C.; Albalak, R. J.; Thomas, E. L. *Macromolecules* **1994**, *27*, 490.
(24) Bates, F. S.; Koppi, K. A.; Tirrell, M.; Almdal, K.; Mortensen, K. *Macromolecules* **1994**, *27*, 5934.
(25) Sakurai, S.; Momii, T.; Taie, K.; Shibayama, M.; Nomura, S.; Hashimoto, T. *Macromolecules* **1993**, *26*, 485.
(26) Wang, H.; Kesani, P. K.; Balsara, N. P.; Hammouda, B. *Macromolecules* **1997**, *30*, 982.
(27) Mortensen, K.; Almdal, K.; Bates, F. S.; Koppi, K.; Tirrell, M.; Norden, B. *Physica B* **1995**, *213*, 682.
(28) Kossuth, M. B.; Morse, D. C.; Bates, F. S. *J. Rheol.* **1999**, *43*, 167.
(29) Ryu, C. Y.; Lee, M. S.; Hajduk, D. A.; Lodge, T. P. *J. Polym. Sci., Polym. Phys. Ed.* **1997**, *35*, 2811.
(30) Kim, J. K., personal communication.
(31) Lodge, T. P.; Pan, C.; Jin, X.; Zhao, Z.; Maurer, W. W.; Bates, F. S. *J. Polym. Sci., Polym. Phys. Ed.* **1995**, *33*, 2289.
(32) Olvera de la Cruz, M. *Phys. Rev. Lett.* **1991**, *67*, 85.
(33) Leibler, L. *Macromolecules* **1980**, *13*, 1602.
(34) Matsen, M. W.; Bates, F. S. *J. Polym. Sci., Polym. Phys. Ed.* **1997**, *35*, 945.
(35) Sakamoto, N.; Hashimoto, T.; Han, C. D.; Kim, D.; Vaidya, N. Y. *Macromolecules* **1997**, *30*, 1621.
(36) Ryu, C. Y. Ph.D. Thesis, University of Minnesota, Minneapolis, MN, 1998.

MA990914+